COLOR DIPOLE BFKL–REGGE FACTORIZATION AND HIGH-ENERGY PHOTON–PHOTON SCATTERING

N. N. Nikolaev[a,b][*], *J. Speth*[a], *V. R. Zoller*[c][**]

[a] *Institut für Kernphysik, Forschungszentrum Jülich*
D-52425, Jülich, Germany

[b] *L. D. Landau Institute for Theoretical Physics*
142432, Chernogolovka, Moscow Region, Russia

[c] *Institute for Theoretical and Experimental Physics*
117218, Moscow, Russia

Based on the color dipole representation, we investigate consequences for the $\gamma^*\gamma^*$, $\gamma^*\gamma$ scattering of the finding by Fadin, Kuraev, and Lipatov that the incorporation of asymptotic freedom into the BFKL equation makes the QCD pomeron a series of isolated poles in the angular momentum plane. The emerging color dipole BFKL–Regge factorization allows us to relate in a model-independent way the contributions of each BFKL pole to the $\gamma^*\gamma^*$, $\gamma^*\gamma$ scattering and the deep inelastic scattering on protons. Numerical predictions based on our early work on the color dipole BFKL phenomenology of the deep inelastic scattering on protons gives a good agreement with the recent experimental data from OPAL and L3 experiments at LEP200. We discuss the role of nonperturbative dynamics and predict a pronounced effect of the Regge-factorization breaking due to large unfactorizable nonperturbative corrections to the perturbative vacuum exchange. We comment on the salient features of the BFKL–Regge expansion for the $\gamma^*\gamma^*$, $\gamma^*\gamma$ scattering including the issue of the decoupling of subleading BFKL poles and the soft plus rightmost hard BFKL pole dominance.

PACS: 12.38.-t, 13.60.Hb, 13.85.Lg

1. INTRODUCTION

We study the scattering of virtual and real photons,

$$\gamma^*(q) + \gamma^*(p) \to X, \tag{1}$$

in the high-energy regime of a large Regge parameter $1/x$; this parameter depends on virtualities of photons as

$$\frac{1}{x} = \frac{W^2 + Q^2 + P^2}{Q^2 + P^2 + \mu^2} \gg 1 \tag{2}$$

and has the correct parton model limit if either $Q^2 \ll P^2$ or $P^2 \ll Q^2$. In Eq. (2), $W^2 = (q+p)^2$ is the center-of-mass energy squared of colliding space-like photons $\gamma^*(q)$ and $\gamma^*(p)$ with the respective virtualities $q^2 = -Q^2$ and $p^2 = -P^2$.

The high-energy virtual photon–virtual photon scattering can be viewed as an interaction of small size color dipoles from the beam and target photons. The recent strong theoretical [1–5] and experimental [1, 6–9] (see also a compilation in [10]) interest in the high-energy $\gamma^*\gamma^*$, $\gamma^*\gamma$, $\gamma\gamma$ scattering stems from the fact that virtualities of photons give a handle on the size of color dipoles in the beam and target photons and, eventually, the short-distance properties of the QCD pomeron exchange. For the earlier development of the subject, see the pioneering paper [11].

As noticed by Fadin, Kuraev, and Lipatov in 1975 [12] and discussed in more detail by Lipatov in [13], the incorporation of the asymptotic freedom into the BFKL equation [14] makes the QCD pomeron a series of isolated poles in the angular-momentum plane. The contribution of each isolated pole to the high-energy scattering amplitude satisfies the familiar Regge factorization [15]. In [16], we reformulated the conse-

[*]E-mail: kph154@ikp301.ikp.kfa-juelich.de
[**]E-mail: zoller@heron.itep.ru

quences of the Regge factorization in our color dipole (CD) approach to the BFKL pomeron. In this paper, we address several closely related issues in the photon–photon scattering in Regge regime (2) which can be tested at LEP200 and Next Linear Collider (NLC).

First, following our early work [16–18], we discuss how the CD BFKL–Regge factorization leads to parameter-free predictions for the total cross sections of the $\gamma^*\gamma^*$, $\gamma^*\gamma$, and $\gamma\gamma$ scattering. We find good agreement with the recent experimental data from the L3 and OPAL experiments at LEP [6–9].

Second, we discuss the interplay of soft and hard dynamics of the vacuum exchange and comment on the onset of the soft plus rightmost hard BFKL-pole dominance in the $\gamma^*\gamma^*$ diffractive scattering. The nodal properties of eigenfunctions of the color dipole BFKL equation suggest an interesting possibility of the decoupling of subleading BFKL singularities when the virtuality of one or both of photons is in the broad vicinity of $Q^2 \sim 20$ GeV^2. This makes the leading hard plus soft approximation (LHSA) previously advocated by us in [18] very efficient.

Third, we discuss the impact of the CD BFKL expansion on the contentious issue of testing the factorization properties of photon–photon scattering in the Q^2, P^2-plane which was previously discussed [4] only in the $\alpha_S = $ const approximation to the BFKL equation. Our result is that the nonperturbative corrections break down the Regge factorization. The experimental observation of this phenomenon would contribute to better understanding of the nonperturbative dynamics of high-energy processes.

2. OVERVIEW OF THE COLOR DIPOLE BFKL–REGGE FACTORIZATION

In the color dipole basis, the beam–target scattering is viewed as a transition of γ^* into a quark–antiquark pair and the interaction of the beam (b) and target (t) color dipoles of the flavor $A, B = u, d, s, c$. As a fundamental quantity, we use the forward dipole scattering amplitude and/or the dipole–dipole cross section $\sigma(x, \mathbf{r}, \mathbf{r}')$. Once $\sigma(x, \mathbf{r}, \mathbf{r}')$ is known, the total cross section of scattering of an $A\overline{A}$ color dipole in the beam on a $B\overline{B}$ color dipole in the target, $\sigma^{AB}(x)$, is calculated as

$$\sigma^{AB}(x) = \int dz d^2\mathbf{r} dz' d^2\mathbf{r}' |\Psi_A(z, \mathbf{r})|^2 \times$$
$$\times |\Psi_B(z', \mathbf{r}')|^2 \sigma(x, \mathbf{r}, \mathbf{r}'), \quad (3)$$

where $\mathbf{r}$ and $\mathbf{r}'$ are the two-dimensional vectors in the impact parameter plane. In the color dipole factorization formula (3), the dipole–dipole cross section $\sigma(x, \mathbf{r}, \mathbf{r}')$ is beam–target symmetric and universal for all beams and targets, the beam and target dependence is concentrated in the probabilities $|\Psi_A(z, \mathbf{r})|^2$ and $|\Psi_B(z', \mathbf{r}')|^2$ to find an $A\overline{A}$ color dipole with $\mathbf{r}$ in the beam and a $B\overline{B}$ color dipole with $\mathbf{r}'$ in the target, respectively. Hereafter, we focus on cross sections averaged over polarizations of the beam and target photons, in which case only the $n = 0$ term of the Fourier series,

$$\sigma(x, \mathbf{r}, \mathbf{r}') = \sum_{n=0}^{\infty} \sigma_n(x, r, r') \exp(in\varphi), \quad (4)$$

where φ is the azimuthal angle between $\mathbf{r}$ and $\mathbf{r}'$, contributes in (3).

In 1975, Fadin, Kuraev, and Lipatov observed [12] (see also Lipatov's extensive discussion [13]) that the incorporation of asymptotic freedom into the BFKL equation makes the QCD pomeron a series of isolated poles in the angular momentum plane. The contribution of each pole to scattering amplitudes satisfies the standard Regge factorization [15], which in the CD basis implies the CD BFKL–Regge expansion for the vacuum exchange dipole–dipole cross section:

$$\sigma(x, r, r') = \sum_m C_m \sigma_m(r) \sigma_m(r') \left(\frac{x_0}{x}\right)^{\Delta_m}. \quad (5)$$

Here, the dipole cross section $\sigma_m(r)$ is an eigenfunction of the CD BFKL equation [16, 17, 19–21]

$$\frac{\partial \sigma_m(x, r)}{\partial \ln(1/x)} = \mathcal{K} \otimes \sigma_m(x, r) = \Delta_m \sigma_m(x, r), \quad (6)$$

with the eigenvalue (intercept) Δ_m, where $\mathcal{K}$ is the kernel of the BFKL equation in the CD representation [16]. Arguably, for the transition of γ^* into heavy flavors, with $A = c, b, \ldots$, the hardness scale is set by $Q^2 + 4m_A^2$, and for light flavors, $Q^2 + m_\rho^2$ is a sensible choice. Hence, for the light–light transition, we evaluate Regge parameter (2) with $\mu^2 = m_\rho^2$, for the light-charm contribution, we take $\mu^2 = 4m_c^2$, and for the charm–charm contribution, we take $\mu^2 = 8m_c^2$.

We refer to our early works [16, 17, 21] for the details on the CD formulation of the BFKL equation, the infrared regularization by a finite propagation radius R_c for perturbative gluons and the freezing of strong coupling at large distances, the choice of the physically motivated boundary condition for the hard BFKL evolution, and for the description of eigenfunctions. The successful application of the CD BFKL–Regge expansion to the proton and pion structure functions and

the evaluation of the hard-pomeron contribution to the rise of hadronic and real photoabsorption cross sections can be found in [16–18, 21]. We only recapitulate the salient features of the formalism that are essential for the present discussion.

There is a useful analogy between the intercept $\Delta = \alpha(0) - 1$ and the binding energy for the bound state problem for the Schrödinger equation. The eigenfunction $\sigma_0(r)$ for the rightmost hard BFKL pole (the ground state) corresponding to the largest intercept $\Delta_0 \equiv \Delta_{\mathbb{P}}$ is node-free. The eigenfunctions $\sigma_m(r)$ for excited states with m radial nodes have the intercept $\Delta_m < \Delta_{\mathbb{P}}$. Our choice of $R_c = 0.27$ fm yields the intercept $\Delta_{\mathbb{P}} = 0.4$ for the rightmost hard BFKL pole and $\Delta_m \approx \Delta_0/(m+1)$ for subleading hard poles. The node of $\sigma_1(r)$ is located at $r = r_1 \approx 0.05$–0.06 fm, for larger m the rightmost nodes move to a somewhat larger r and accumulate at $r \sim 0.1$ fm; see [16, 17] for a more detailed description of the nodal structure of $\sigma_m(r)$. Here we only emphasize that for solutions with $m \geq 3$, the third and higher nodes are located at a very small r far beyond the resolution scale $1/\sqrt{Q^2}$ of foreseeable deep inelastic scattering (DIS) experiments. We note that the Regge cut in the complex angular momentum plane found in the much discussed approximation $\alpha_S = $ const resembles an infinite, and continuous, sequence of poles. In a counterpart of our CD BFKL–Regge expansion (5) for the approximation $\alpha_S = $ const, the intercept Δ_m would be a continuous parameter in contrast to the discrete spectrum for the standard running α_S parameter.

Because the BFKL equation sums cross sections of the production of multigluon final states, the perturbative two-gluon Born approximation is an arguably natural boundary condition. This leaves the starting point x_0 as the only free parameter that completely fixes the result of the hard BFKL evolution for the dipole–dipole cross section. We follow the choice $x_0 = 0.03$ made in [21]. The very ambitious program for describing $F_{2p}(x, Q^2)$ starting from this, perhaps excessively restrictive, perturbative two-gluon boundary condition has been launched by us in [16] and met with remarkable phenomenological success [17, 18].

Because the subleading solutions with $m \geq 3$ cannot be resolved in the attainable region of r and all these solutions have similar intercepts $\Delta_m \ll 1$, in practical evaluation of σ^{AB} we can truncate expansion (5) at $m = 3$, thereby lumping the contributions of all singularities with $m \geq 3$ in the $m = 3$ term. Specifically, if we endow

$$\sigma_3(r) = \sigma_{Born}(r) - \sum_{m=0}^{2} \sigma_m(r) \qquad (7)$$

with the effective intercept $\Delta_3 = 0.06$, the truncated expansion reproduces the numerical solution $\sigma(x, r)$ of our CD BFKL equation in the wide range of dipole sizes 10^{-3} fm $\lesssim r \lesssim 10$ fm with the accuracy of approximately 10% even at moderately small x. This truncation can be justified a *posteriori* if the contribution from $m \geq 3$ turns out to be a small correction, which is indeed the case at small x.

Whereas the scattering of small dipoles $r \lesssim R_c$ is dominated by the exchange of perturbative gluons, the interaction of large dipoles with the proton target has been modeled in Ref. [17, 18, 21] by the nonperturbative soft pomeron with the intercept $\alpha_{soft}(0) - 1 = \Delta_{soft} = 0$. An extra term $\sigma_{soft}(r, r')$ must then be added to the right-hand side of expansion (5).

From the early phenomenology of DIS and the diffractive vector meson production off the proton target, we only know the parameterization of $\sigma_{soft}(r, r')$ when one of the dipoles is definitely large, of the order of the proton size. Evaluation of the soft contribution to the $\gamma^*\gamma^*$ scattering inevitably introduces model dependence if both dipoles are small. Modeling the soft contribution by the exchange of two nonperturbative gluons suggests [22]

$$\sigma_{soft}(r, r') \propto \frac{r^2 r'^2}{r^2 + r'^2}$$

and the nonfactorizable cross section in the form

$$\sigma_{soft}^{\gamma^*\gamma^*}(Q^2, P^2) \propto \frac{1}{Q^2 + P^2}.$$

A similar nonperturbative cross section σ_{soft} is found in the soft pomeron models [23]. The explicit parameterization is given in Appendix.

Finally, at moderately small values of x, the t-channel gluon tower exchange described above must be complemented by the t-channel $q\bar{q}$ exchange often associated with the DIS off vector mesons (hadronic component) and off the perturbative (point-like) $q\bar{q}$-component of the target photon wave function. We add the corresponding corrections only to the real photon structure function $F_{2\gamma}(x, Q^2)$ to estimate the interplay of the vacuum and nonvacuum exchanges in the currently accessible kinematical region of not very small x. In all other cases of interst, we concentrate on the pure vacuum exchange at $x \lesssim x_0$, where the nonvacuum corrections are negligibly small.

In our evaluation of the box diagram contribution to $F_{2\gamma}^{pl}(x, Q^2)$, which is [24]

$$F_{2\gamma}^{pl}(x, Q^2) = \frac{3\alpha_{em}}{\pi} \sum_{q=u,d,s,c} e_q^4 x \left\{ \left[x^2 + (1-x)^2 \right] \times \right. $$
$$\left. \times \ln \frac{Q^2(1-x)}{xQ_q^2} + 8x(1-x) - 1 \right\}, \quad (8)$$

we take the ρ-meson mass as the lower cut-off for the light-flavor-loop integral, $Q_q^2 = m_\rho^2$ for $q = u, d, s$, and the charm quark mass for the c-loop, $Q_c^2 = m_c^2$. In Eq. (8), e_q is the quark charge.

To describe the hadronic component of $F_{2\gamma}$ we take the coherent mixture of the ρ^0 and ω mesons [25]. Supplemented with the standard assumptions on the vector meson valence quark density, this gives

$$F_{2\gamma}^{had}(x) = \frac{\alpha_{em}}{12} \left[4(g_\rho + g_\omega)^2 + (g_\rho - g_\omega)^2) \right] \times $$
$$\times \sqrt{x}\,(1-x), \quad (9)$$

where the coupling constants $g_V^2 = 4\pi/f_V^2$ entering the Fock state expansion

$$|\gamma\rangle^{had} = \frac{e}{f_\rho}|\rho\rangle + \frac{e}{f_\omega}|\omega\rangle + \ldots$$

are given by $g_\rho^2 = 0.5$ and $g_\omega^2 = 0.043$ [10]. We neglect the Q^2 evolution which, at reasonable values of the lower scale, is a small correction on the interval $1.9 \text{ GeV}^2 \leq Q^2 \leq 5 \text{ GeV}^2$ where the small-x data on $F_{2\gamma}$ were taken.

Combining Eqs. (5) and (3) and adding the soft and nonvacuum components, we obtain our principal result for the virtual–virtual scattering ($m = 0, 1, 2, 3$, $A, B = u, d, s, c$)

$$\sigma_{vac}^{\gamma^*\gamma^*}(x, Q^2, P^2) = \frac{(4\pi^2\alpha_{em})^2}{Q^2 P^2} \times $$
$$\times \sum_m C_m \sum_{A,B} f_m^A(Q^2) f_m^B(P^2) \left(\frac{3x_0}{2x_{AB}} \right)^{\Delta_m} + $$
$$+ \sigma_{soft}^{\gamma^*\gamma^*}(x, Q^2, P^2). \quad (10)$$

To make the scale dependence discussed in Introduction explicit, we provide μ and x defined by Eq. (2) with two indices, A and B, indicating the flavor of the beam and the target dipoles: $\mu_{AB}^2 = m_\rho^2$ for $A, B = u, d, s$ while $\mu_{AB}^2 = 4m_c^2$ if either $A = c$ or $B = c$ and the second dipole is made of light quarks and $\mu_{AB}^2 = 8m_c^2$ if $A = B = c$.

For the DIS off real (quasi-real) photons with $P^2 \approx 0$ we have ($A = u, d, s, c$)

$$F_{2\gamma}(x, Q^2) = \sum_m A_m^\gamma \sum_A f_m^A(Q^2) \left(\frac{3}{2} \frac{x_0}{x_A} \right)^{\Delta_m} + $$
$$+ F_{2\gamma}^{soft}(x, Q^2) + F_{2\gamma}^{nvac}(x, Q^2), \quad (11)$$

where

$$x_A = \frac{Q^2 + \mu_A^2}{W^2 + Q^2}$$

and $\mu_A^2 = m_\rho^2$ for $A = u, d, s$, while $\mu_A^2 = 4m_c^2$ for $A = c$. The $c\bar{c}$ component of the target photon wave function is strongly suppressed at $P^2 \approx 0$ and can be neglected for all the practical purposes as well as the $c\bar{c}$ content of the target proton. This observation simplifies factorization relation (11) for the real photon structure function. In Eq. (11), the nonvacuum component denoted by $F_{2\gamma}^{nvac}$ is

$$F_{2\gamma}^{nvac}(x, Q^2) = F_{2\gamma}^{had}(x, Q^2) + F_{2\gamma}^{pl}(x, Q^2) \quad (12)$$

and the cross sections

$$\sigma_m^{\gamma^*}(Q^2) = \langle \gamma_T^* | \sigma_m(r) | \gamma_T^* \rangle + \langle \gamma_L^* | \sigma_m(r) | \gamma_L^* \rangle \quad (13)$$

are calculated with the well-known color dipole distributions in the transverse (T) and longitudinal (L) photon of the virtuality Q^2 derived in [26], and the eigen-structure functions are defined as usual,

$$f_m(Q^2) = \frac{Q^2}{4\pi^2\alpha_{em}} \sigma_m^{\gamma^*}(Q^2). \quad (14)$$

The Regge parameter involves the factor $3/2$ because in the scattering of a color dipole on the photon, the effective dipole–dipole collision energy is $3/2$ of that in the reference scattering of the color dipole on the three-quark nucleon at the same total c.m.s. energy W. The analytical formulas for the eigen-structure functions $f_m(Q^2)$ and $f_m^c(Q^2)$ are given in Appendix. Here, as in all our previous calculations, we put $m_c = 1.5$ GeV. We do not need any new parameters in addition to those used in the description of the DIS and real photoabsorption on protons [16–18]; the results for the expansion parameters A_m^γ and $\sigma_m^\gamma(0)$ are summarized in Table 1.

We recall that because of the diffusion in the color dipole space, the exchange of perturbative gluons also contributes to the interaction of large dipoles $r > R_c$ [20]. However, this hard interaction-driven effect is still small at a moderately large Regge parameter. For this reason, we refer to the terms with $m = 0, 1, 2, 3$ as the hard contribution as opposed to the genuine soft interaction.

Table 1.   CD BFKL–Regge expansion parameters

m	Δ_m	σ_m^p, mb	C_m, mb^{-1}	A_m^γ/α_{em}	σ_m^γ, μb	$\sigma_m^{\gamma\gamma}$, nb
0	0.402	1.243	0.804	0.746	6.767	36.84
1	0.220	0.462	2.166	0.559	1.885	7.69
2	0.148	0.374	2.674	0.484	1.320	4.65
3	0.06	3.028	0.330	0.428	9.456	29.53
soft	0	31.19	0.0321	0.351	79.81	204.2

Fig. 1. The normalized ratio of the soft-to-rightmost-hard and subleading hard-to-rightmost hard expansion coefficients ($m = 0, 1, 2, 3, soft$) $r_m(Q^2) = \sigma_m^{\gamma^*\gamma^*}/\sigma_{vac}^{\gamma^*\gamma^*}$ of the BFKL–Regge expansion for the $\gamma^*\gamma^*$ scattering at $x = x_0$

Fig. 2. Predictions from the CD BFKL–Regge expansion for the effective intercept Δ_{eff}, Eq. (15), for the diagonal case $Q^2 = P^2$ and $W = 50$ GeV (dotted curve), 100 GeV (dashed curve), 200 GeV (dot-dashed curve)

3. ISOLATING THE SOFT PLUS RIGHTMOST HARD BFKL POLE IN HIGHLY VIRTUAL–VIRTUAL $\gamma^*\gamma^*$ SCATTERING

We start with the theoretically cleanest case of the highly virtual photons, $P^2, Q^2 \gg 1$ GeV^2, and focus on the vacuum exchange component of the total cross section. The CD BFKL approach with asymptotic freedom uniquely predicts that subleading eigen-structure functions have a node at $Q^2 \sim 20$ GeV^2; in this region of Q^2, the rightmost hard pole contribution dominates. This suppression of the subleading hard background is shown in Fig. 1, where we plot the ratio ($m = 0, 1, 2, 3, soft$)

$$r_m(Q^2) = \frac{\sigma_m^{\gamma^*\gamma^*}\left(\frac{3}{2}x_0, Q^2, Q^2\right)}{\sigma_{vac}^{\gamma^*\gamma^*}\left(\frac{3}{2}x_0, Q^2, Q^2\right)}$$
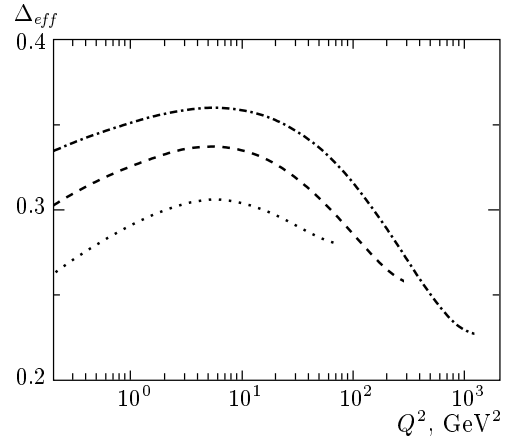
that defines the relative size of different contributions to $\sigma_{vac}^{\gamma^*\gamma^*}$ at $x = 3x_0/2$. At this value of x, the contribution of the subleading hard BFKL poles remains marginal in a broad range of Q^2, although the contribution of the single-node component $m = 1$ becomes substantial at $Q^2 \gtrsim 10^3$ GeV^2.

The soft-pomeron exchange contributes substantially over all Q^2 and dominates at $Q^2 \lesssim 1$ GeV^2. However, at very large $W \sim 100$ GeV, which is of the practical interest at LEP and LHC, such small values of Q^2 correspond to very small x, where the soft and subleading hard contributions are Regge suppressed by the factor $(x/x_0)^{\Delta_\mathbb{P}}$ and $(x/x_0)^{0.5\Delta_\mathbb{P}}$, respectively. The latter is clearly seen in Fig. 2, where the effective pomeron intercept

$$\Delta_{eff} = -\frac{\partial \ln \sigma_{vac}^{\gamma^*\gamma^*}}{\partial \ln x} \qquad (15)$$
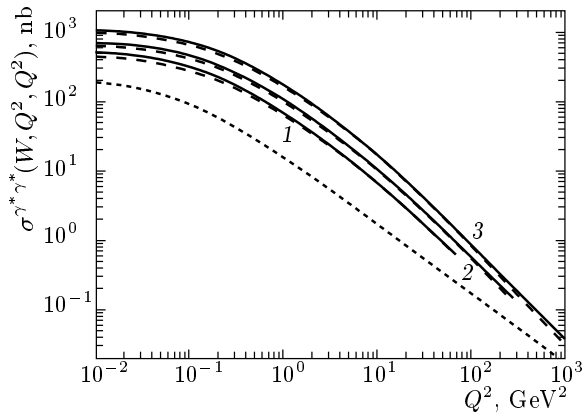
Fig. 3. Predictions from the CD BFKL–Regge expansion for the vacuum exchange component of the virtual–virtial $\gamma^*\gamma^*$ cross section for the diagonal case of $Q^2 = P^2$ and for the cms collision energy $W = 50$, 100 and 200 GeV (solid curves 1, 2, and 3, respectively). The leading hard BFKL exchnage plus soft-pomeron exchange Approximation (LHSA) is shown by the long-dash curve. The soft pomeron component of the cross section is shown separately by the dashed curve

is presented for the diagonal case $Q^2 = P^2$ at three different values of W.

According to the results shown in Fig. 1, the dominance of the soft plus rightmost hard BFKL pomeron exchange in the virtual–virtual $\gamma^*\gamma^*$ scattering holds in a very broad range of $Q^2, P^2 \lesssim 500 \,\mathrm{GeV}^2$, which nearly exhausts the interesting kinematical region at LEP200 and NLC. The quality of the leading hard pole plus soft approximation (LHSA) can also be judged from Fig. 3 for the diagonal case where $Q^2 = P^2$; in Fig. 3 we show the soft component of the cross section separately (the dashed curve). That the contribution of the subleading hard BFKL exchange is marginal is clear from the finding that the approximation of a soft pomeron plus the rightmost hard BFKL exchange (LHSA) shown by long-dash curve nearly exhausts the result of the complete CD BFKL–Regge expansion for the vacuum exchange.

Recently, the L3 collaboration [8] reported the first experimental evaluation of the vacuum exchange in the equal virtuality $\gamma^*\gamma^*$ scattering. Their procedure of subtracting the nonvacuum reggeon and/or the quark parton model contribution is described in [8], arguably the subtraction uncertainties are marginal within the present error bars. In Fig. 4, we compare our predictions to the L3 data. The experimental data and theoretical curves are shown vs. the variable $Y = \ln(W^2/\sqrt{Q^2 P^2})$. The

virtuality of two photons varies in the range of $1.2 \,\mathrm{GeV}^2 < Q^2, P^2 < 9 \,\mathrm{GeV}^2$ ($\langle Q^2, P^2 \rangle = 3.5 \,\mathrm{GeV}^2$) at $\sqrt{s} \approx 91 \,\mathrm{GeV}$ and $2.5 \,\mathrm{GeV}^2 < Q^2, P^2 < 35 \,\mathrm{GeV}^2$ at $\sqrt{s} \approx 183 \,\mathrm{GeV}$ ($\langle Q^2, P^2 \rangle = 14 \,\mathrm{GeV}^2$). We applied the averaging procedure described in [8] to the theoretical cross sections. The solid curve is a result of the complete BFKL–Regge expansion for the vacuum exchange, the long-dash curve is a sum of the rightmost hard BFKL exchange and the soft-pomeron exchange. Shown by the dashed line is the soft pomeron contribution. The agreement of our estimates with the experiment is good, the contribution of the subleading hard BFKL exchange is negligible within the experimental error bars.

The early calculations [2–4] of the perturbative vacuum component of $\sigma^{\gamma^*\gamma^*}$ used the approximation $\alpha_S = \mathrm{const}$ that predicts the P^2, Q^2-dependence different from our result for the CD BFKL approach with running α_S. A detailed comparison with numerical results by Brodsky, Hautmann, and Soper (BHS) [4] is reported by the L3 Collaboration [8], which founds that BHS formulas substantially overpredict $\sigma^{\gamma^*\gamma^*}_{vac}$. In [3], the same perturbative fixed-α_S BFKL model with a massive c-quark was considered. At $\langle Q^2 \rangle = 14 \,\mathrm{GeV}^2$ and moderately small x ($x \gtrsim 3 \cdot 10^{-2}$), the model is in agreement with the L3 data, but at smaller x, already at $x \approx 7 \cdot 10^{-3}$, it substanially overpredicts $\sigma^{\gamma^*\gamma^*}_{vac}$. At $\langle Q^2 \rangle = 3.5 \,\mathrm{GeV}^2$, the results in [3] are substantially above the L3 data for all x.

4. VIRTUAL–REAL $\gamma^*\gamma$ SCATTERING: THE RIGHTMOST HARD BFKL POLE IN THE PHOTON STRUCTURE FUNCTION

The discussion of the photon structure function closely follows that of the proton and pion structure functions in [16–18]. Our normalization of eigenfunctions is such that the vacuum (sea) contribution to the proton structure function ($m = soft, 0, 1, \ldots, 3$)

$$F_{2p}(x, Q^2) = \sum_m f_m(Q^2) \left(\frac{x_0}{x}\right)^{\Delta_m}, \qquad (16)$$

has the CD BFKL–Regge expansion coefficients $A^p_m = 1$. There is a fundamental point that the distribution of small-size color dipoles in the photon is enhanced compared to that in the proton [18]; this enhances the importance of the rightmost hard BFKL exchange. Indeed, closer inspection of the expansion coefficients A^γ_m shown in table 1 reveals that subleading hard BFKL exchanges are suppressed by the factor ~ 1.5 to 2, whereas the soft-pomeron exchange contribution is suppressed by the factor ~ 3.
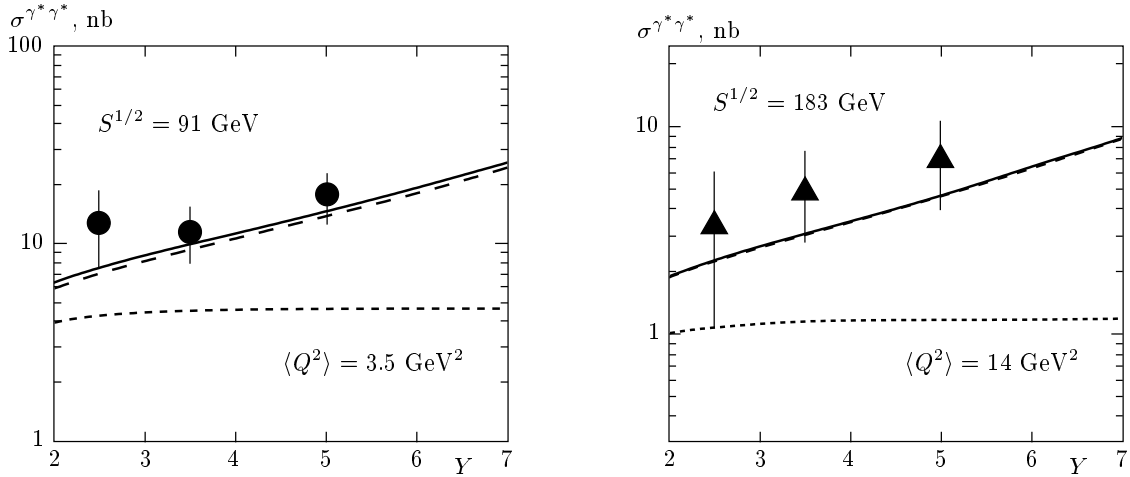
Fig. 4. Predictions from the CD BFKL–Regge expansion for the vacuum exchange component of the virtual–virtial $\gamma^*\gamma^*$ cross section for the diagonal case of $\langle Q^2 \rangle = \langle P^2 \rangle$ are confronted with the experimental data by the L3 Collaboration [10]. The experimental data and theoretical curves are shown vs. the variable $Y = \ln(W^2/\sqrt{Q^2 P^2})$
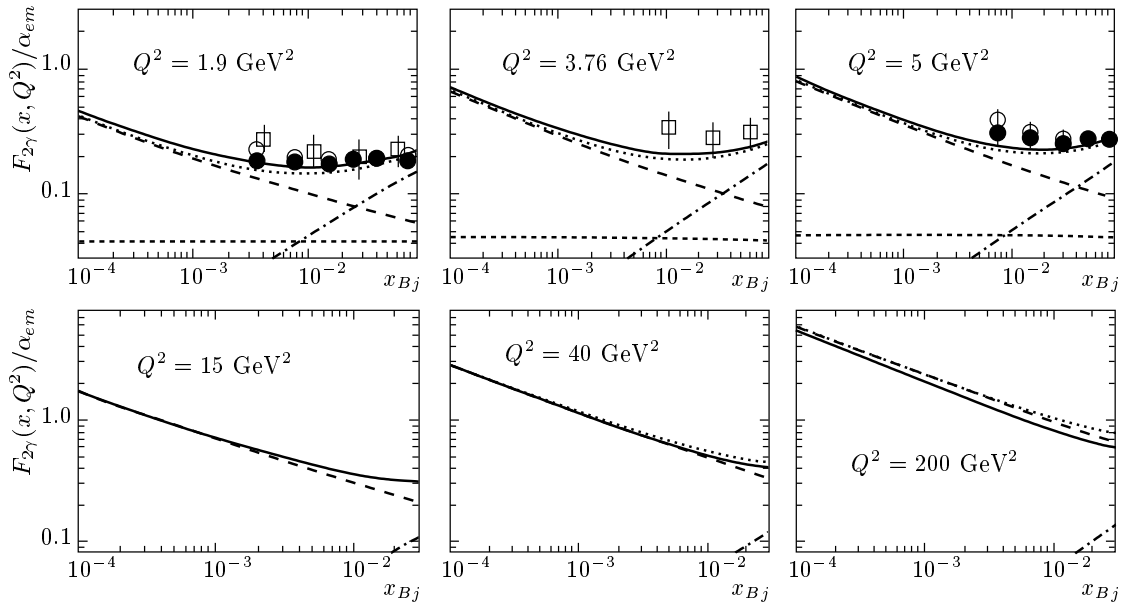

Fig. 5. Predictions from the CD the BFKL–Regge expansion for the photon structure function. The solid curve shows the result from the complete BFKL–Regge expansion with the soft-pomeron (the dashed curve) and valence (the dot-dashed curve) components included, the dotted curve shows the rightmost hard BFKL (LH) plus soft-pomeron (S) plus non-vacuum (NV) approximation (LHSNVA). The long-dash line corresponds to the LH plus S approximation (LHSA). Data points are from [6, 9]

Our predictions for the photon structure function are parameter-free and are presented in Fig. 5. At moderately small $x \sim 0.1$, there is a substantial nonvacuum reggeon exchange contribution from the DIS off the hadronic ($q\bar{q}$) component of the target photon wave function, which can be regarded as well constrained by

the large x data. We use here the parameterizations presented above (Eqs. (8), (9), and (12)). The solid curve shows the result of the complete BFKL–Regge expansion with the soft-pomeron (the dashed curve) and quasi-valence (the dot-dashed curve) components included, the dotted curve shows the rightmost hard
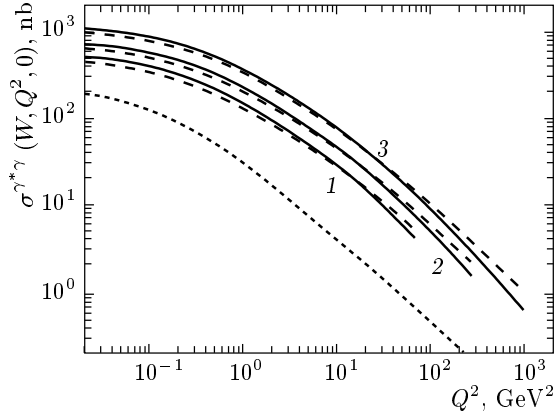
Fig. 6. Predictions from the CD BFKL–Regge expansion for the vacuum exchange component of the the virtual–real $\gamma^*\gamma$ total cross section and for the cms collision energy $W = 50$, 100, and 200 GeV (solid curves *1*, *2*, and *3*, respectively). The result from the rightmost hard BFKL (LH) plus soft-pomeron (S) approximation (LHSA) is shown by the long-dash curve. The soft-pomeron exchange component of the cross section is shown separately by the dashed curve

BFKL (LH) plus soft-pomeron (S) plus nonvacuum (NV) approximation (LHSNVA). A comparison of the solid and dotted curves clearly shows that the subleading hard BFKL exchanges are numerically small in the experimentally interesting region of Q^2, the rightmost hard BFKL pole exhausts the hard vacuum contribution for $2\ \mathrm{GeV}^2 \lesssim Q^2 \lesssim 100\ \mathrm{GeV}^2$. The nodal properties of subleading hard BFKL structure functions are clearly seen: LHSNVA slightly underestimates $F_{2\gamma}$ at $Q^2 \lesssim 10\ \mathrm{GeV}^2$ and overestimates $F_{2\gamma}$ at $Q^2 \gtrsim 50\ \mathrm{GeV}^2$. For another illustration of the same nodal property of the subleading hard components, see Fig. 6, where we show the vacuum component of the virtual–real total cross section $\sigma^{\gamma^*\gamma}_{tot}$ as a function of Q^2 at fixed W. As seen from Fig. 1, the soft contribution rises towards small Q^2, but this rise is compensated to a large extent by the small-x enhancement of the rightmost hard BFKL contribution by the large Regge factor $(x_0/x)^{\Delta_\mathbb{P}}$. For this region, the soft background (the dashed curve) remains marginal over the entire range of Q^2. Because of the node effect, the $m = 1$ subleading component changes the sign and becomes quite substantial at very large Q^2 and moderately small x.

Recently, the L3 and OPAL collaborations reported the first experimental data on the photon structure function at sufficiently small x [6, 9]. These data are shown in Fig. 5 and are in good agreement with the predictions from the CD BFKL–Regge expansion. A

comparison with the long-dash curve, which is the sum of the rightmost hard BFKL and soft exchanges, shows that the experimental data are in the region of x and Q^2 still affected by the nonvacuum reggeon (quasivalence) exchange; going to smaller x and larger Q^2 would greatly improve the sensitivity to the pure vacuum exchange.

In order to give a crude idea on finite-energy effects at large x and not so large values of the Regge parameter, we stretch the theoretical curves slightly to $x \gtrsim x_0$ by multiplying the BFKL–Regge expansion result with the purely phenomenological factor $1 - x$ motivated by the familiar behavior of the gluon structure function of the photon $\sim (1 - x)^n$ with the exponent $n \sim 1$.

5. THE REAL–REAL $\gamma\gamma$ SCATTERING

We recall that because of the well-known BFKL diffusion in the color dipole space, the exchange by perturbative gluons also contributes to the interaction of large dipoles $r > R_c$ [20]. As discussed in [18], this gives rise to a substantially rising component of the hadronic and real photoabsorption cross sections and a scenario in which the observed rise of hadronic and real photon cross sections are entirely due to this intrusion of hard scattering. This is a motivation behind our choice of the intercept $\Delta_{soft} = 0$ for the soft pomeron exchange. Furthermore, in order to make this picture quantitative, one must invoke strong absorption/unitarization to tame the too rapid growth of the large dipole component of the hard BFKL dipole cross section. The case of the real–real $\gamma\gamma$ scattering is not an exception and the above enhancement of small dipole configurations in photons compared to hadrons uniquely predicts that the hard BFKL exchange component of the real–real $\gamma\gamma$ scattering is enhanced compared to the proton–proton and/or pion–proton scattering. This is clearly seen from Table 1, where we show the coefficients

$$\sigma^{\gamma\gamma}_m = \sigma^\gamma_m \sigma^\gamma_m C_m \qquad (17)$$

of the expansion for the vacuum exchange component of the total $\gamma\gamma$ cross section ($m = 0, 1, 2, 3, soft$)

$$\sigma^{\gamma\gamma}_{vac} = \sum_m \sigma^{\gamma\gamma}_m \left(\frac{W^2 x_0}{m^2_\rho} \right)^{\Delta_m} . \qquad (18)$$

One must look at the soft–hard hierarchy of $\sigma^{\gamma\gamma}_m$ and $\sigma^\gamma_m, \sigma^p_m$ in the counterparts of (18) for the γp and pp scattering. This enhancement of the hard BFKL exchange is confirmed by a simplified vacuum pole plus nonvacuum reggeon exchange fits to the real–real $\gamma\gamma$
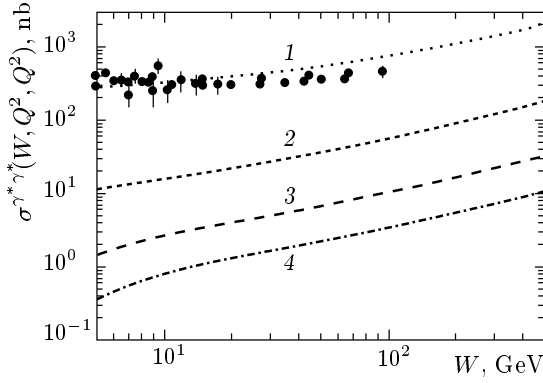
Fig. 7. Our predictions from the CD BFKL–Regge factorization for the single-vacuum exchange contribution to the real–real $\gamma\gamma$ scattering are compared with the recent experimental data from the OPAL collaboration [7] and [10] for the cases of $Q^2 = 0$ (curve *1*), 2 GeV^2 (curve *2*), 10 GeV^2 (curve *3*), 25 GeV^2 (curve *4*)

Fig. 8. Our evaluation of $R_{\gamma\gamma}$ for single-vacuum component of total cross sections using the CD BFKL approach (solid curve) and the rightmost hard BFKL plus soft-pomeron approximation (LHSA, dashed curve)

total cross section: the found intercept of the effective vacuum pole, $\epsilon^{\gamma\gamma} \approx 0.21$, is much larger than $\epsilon \approx 0.095$ from similar fits to the hadronic cross section data. In Fig. 7, we compare our predictions from the CD BFKL–Regge factorization for the single-vacuum exchange contribution to the real–real $\gamma\gamma$ scattering with the recent experimental data from the OPAL collaboration [7] and [10]. The theoretical curves are in the right ballpark, but the truly quantitative discussion of total cross sections of soft processes requires better understanding of the absorption/unitarization effects.

6. REGGE FACTORIZATION IN THE $\gamma^*\gamma^*$ AND $\gamma\gamma$ SCATTERING

If the vacuum exchange were an isolated Regge pole, the well-known Regge factorization would hold for asymptotic cross sections [15],

$$\sigma_{tot}^{bb}\sigma_{tot}^{aa} = \sigma_{tot}^{ab}\sigma_{tot}^{ab}. \tag{19}$$

In the CD BFKL approach, this Regge factorization holds for each term in the BFKL–Regge expansion for the vacuum exchange, but evidently the sum of the factorized terms does not satisfy factorization (19). One can hope for an approximate factorization if a single term dominates the BFKL–Regge expansion. The corrections to the exact factorization still exist even for the single pole exchange because of the light $q\bar{q}$ and charm $c\bar{c}$ mass scale difference discussed above.

One such case is the real–real $\gamma\gamma$ scattering dominated by the soft-pomeron exchange (although the
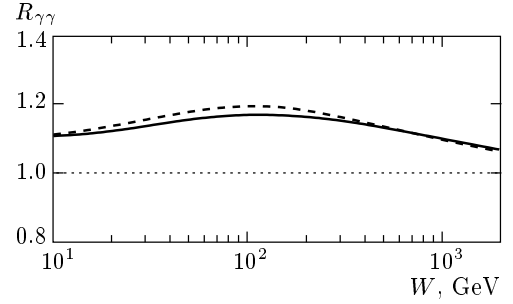
factorization of the soft on-shell amplitudes never gained strong support from the high-energy Regge phenomenology). For this reason, the CD BFKL–Regge expansion, that reproduces well the vacuum exchange components of the pp and γp scattering cannot fail for the vacuum component in real–real $\gamma\gamma$ scattering. The rise of the contribution of the hard-BFKL exchange breaks the Regge factorization relation

$$R_{\gamma\gamma} = \frac{\sigma_{vac}^{\gamma\gamma}\sigma^{pp}}{\sigma_{vac}^{\gamma p}\sigma_{vac}^{\gamma p}} = 1, \tag{20}$$

which would restore at extremely high energies such that the rightmost hard BFKL exchange dominates. This property is illustrated in Fig. 8, where we show our evaluation of R for the single-vacuum component of the total cross sections entering (19). At moderately high energies, the naive factorization breaks but the expected breaking is still weak, $\lesssim 20\%$. This curve must not be taken at face value for $W \gtrsim 0.1$–1 TeV because of likely strong absorption effects, but the trend of R being larger than unity and rising with energy should withstand the unitarity effects. The second case is the highly virtual–virtual $\gamma^*\gamma^*$ scattering. As we emphasized in Sec. 3, the CD BFKL approach here uniquely predicts that because of the nodal property of the subleading eigen-structure functions, the superposition of soft and rightmost hard BFKL poles dominate the vacuum exchange in a broad range of $Q^2, P^2 \lesssim 10^3$ GeV^2.

The above discussion clearly suggests that different cross sections must be taken at the same value of $x^{-1} = W^2/(Q^2 + P^2)$, in which case the vacuum components of the $\gamma^*\gamma^*$ scattering at $Q^2, P^2 \gg 4m_c^2$ and $x \ll x_0$ would satisfy

$$R_{\gamma^*\gamma^*}(x) =$$
$$= \frac{[\sigma^{\gamma^*\gamma^*}(x, Q^2, P^2)]^2}{\sigma^{\gamma^*\gamma^*}(x, Q^2, Q^2)\sigma^{\gamma^*\gamma^*}(x, P^2, P^2)} = 1. \tag{21}$$
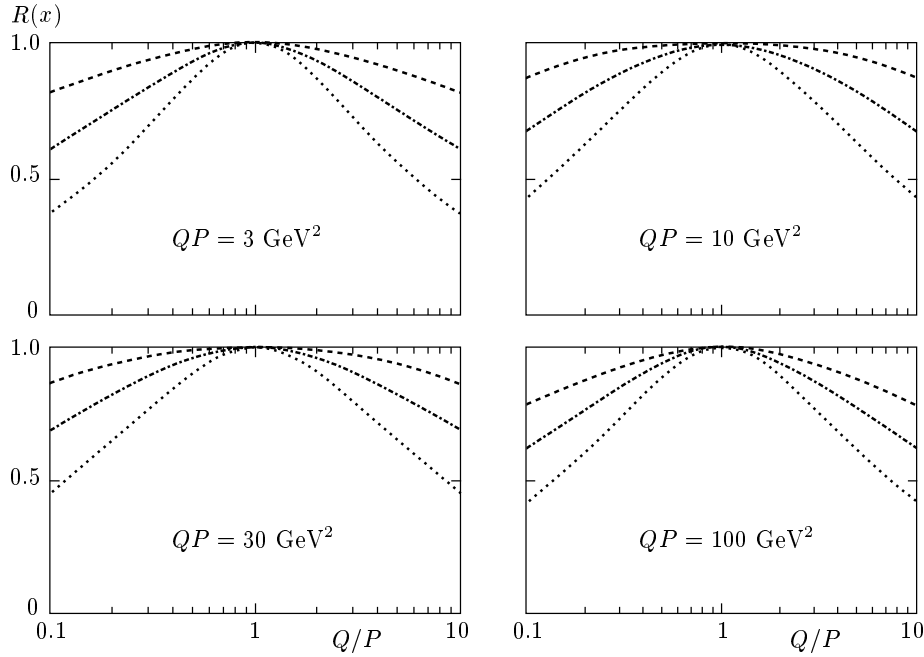
Fig. 9. The factorization cross section ratio $R_{\gamma^*\gamma^*}(x)$ at fixed x and QP as a function of Q/P for $x = 10^{-2}$ (dotted line), $x = 10^{-3}$ (long-dash line), and $x = 10^{-4}$ (dashed line)

In accordance with the results shown in Fig. 1, the soft exchanges break factorization relation (21). The breaking is quite substantial at moderate $x = 0.01$ (dotted line in Fig. 9), and breaking effects disappear rapidly (as x^{Δ_0}) when $x \to 0$. If the vacuum singularity were the Regge cut, as is the case with the approximation $\alpha_S = \text{const}$, the restoration of factorization is much slower, cf. our Fig. 9 and Fig. 9 in [4].

For the obvious reason that the soft-pomeron exchange is so predominant in the real photon scattering, whereas the soft plus rightmost hard BFKL exchange is outstanding in the virtual–virtual and real–virtual photon–photon scattering, it is ill advised to look at factorization ratio $R_{\gamma^*\gamma^*}(W)$ when one of the photons is quasi-real, $P^2 \sim 0$. In this limit, one would find strong departures of $R_{\gamma^*\gamma^*}(W)$ from unity. For precisely the same reason of predominance of the soft-pomeron exchange in the pp scattering vs. a nearly dominant rightmost hard BFKL pole exchange in DIS at small x and 5–10 GeV$^2 \lesssim Q^2 \lesssim 100$ GeV^2, see [18], the naive factorization estimate

$$\sigma^{\gamma^*\gamma^*}(W, Q^2, P^2) \approx \frac{\sigma^{\gamma^* p}(W, Q^2)\sigma^{\gamma^* p}(W, P^2)}{\sigma^{pp}(W)} \quad (22)$$

would not make much sense.

7. CONCLUSIONS

We explored the consequences for small-x photon structure functions $F_{2\gamma}(x, Q^2)$ and high-energy two-photon cross sections $\sigma^{\gamma^*\gamma^*}$ and $\sigma^{\gamma\gamma}$ from the color dipole BFKL–Regge factorization. Because of the nodal properties of eigen-structure functions of subleading hard BFKL exchanges, the CD BFKL approach uniquely predicts that the vacuum exchange is strongly dominated by the combination of soft plus rightmost hard BFKL pole exchanges in a very broad range of photon virtualities Q^2, P^2 which includes much of the kinematical domain attainable at LEP200 and NLC. Starting with a very restrictive perturbative two-gluon exchange as a boundary condition for the BFKL evolution in the color dipole basis and having fixed the staring point of the BFKL evolution in the early resulting CD BFKL–Regge phenomenology of the proton structure finction, we presented parameter-free predictions for the vacuum exchange contribution to the photon structure function that agree well with OPAL and L3 determinations. A good agreement is found between our predictions for the energy and photon virtuality dependence of the photon–photon cross section $\sigma^{\gamma^*\gamma^*}(W, Q^2, P^2)$ and the recent data taken by the L3 Collaboration [8]. We commented on the utility of Regge factorization tests of the CD BFKL–Regge expansion.

Table 2. CD BFKL–Regge the all-flavor structure function parameters

m	a_m	c_m	r_m^2, GeV^{-2}	R_m^2, GeV^{-2}	$z_m^{(1)}$	$z_m^{(2)}$	$z_m^{(3)}$	δ_m
0	0.0232	0.3261	1.1204	2.6018				1.
1	0.2788	0.1113	0.8755	3.4648	2.4773			1.0915
2	0.1953	0.0833	1.5682	3.4824	1.7706	12.991		1.2450
3	1.4000	0.04119	3.9567	2.7706	0.23585	0.72853	1.13044	0.5007
soft	0.1077	0.0673	7.0332	6.6447				

Table 3. CD BFKL–Regge charm structure function parameters

m	a_m	c_m	r_m^2, GeV^{-2}	R_m^2, GeV^{-2}	K_m^2, GeV^{-2}	$z_m^{(1)}$	$z_m^{(2)}$	δ_m
0	0.02140	0.2619	0.3239	0.2846				1.
1	0.0782	0.03517	0.0793	0.2958	0.2846	0.2499		1.9249
2	0.00438	0.03625	0.0884	0.2896	0.2846	0.0175	3.447	1.7985
3	-0.26313	2.1431	$3.7424 \cdot 10^{-2}$	$8.1639 \cdot 10^{-2}$	0.13087	158.52	559.50	0.62563
soft	0.01105	0.3044	0.09145	0.1303				

APPENDIX

A.1. CD BFKL all-flavor eigen-structure functions

In the early discussion of DIS off protons, the results of numerical solutions of the CD BFKL equation for the all-flavor $(u+d+s+c)$ eigen-structure functions $f_m(Q^2)$ were parameterized as

$$f_0(Q^2) = a_0 \frac{R_0^2 Q^2}{1 + R_0^2 Q^2} \times$$
$$\times \left[1 + c_0 \ln(1 + r_0^2 Q^2)\right]^{\gamma_0}, \quad (23)$$

$$f_m(Q^2) = a_m f_0(Q^2) \frac{1 + R_0^2 Q^2}{1 + R_m^2 Q^2} \times$$
$$\times \prod_{i=1}^{m} \left(1 - \frac{z}{z_m^{(i)}}\right), \quad m \geq 1, \quad (24)$$

where $\gamma_0 = 4/3\Delta_0$ and

$$z = \left[1 + c_m \ln(1 + r_m^2 Q^2)\right]^{\gamma_m} - 1, \quad \gamma_m = \gamma_0 \delta_m. \quad (25)$$

The parameters tuned to reproduce the numerical results for $f_m(Q^2)$ at $Q^2 \lesssim 10^5$ GeV^2 are listed in Table 2.

The soft component of the proton structure function as derived from $\sigma_{soft}(r)$ taken from [27] is parameterized as

$$f_{soft}(Q^2) = \frac{a_{soft} R_{soft}^2 Q^2}{1 + R_{soft}^2 Q^2} \times$$
$$\times \left[1 + c_{soft} \ln(1 + r_{soft}^2 Q^2)\right], \quad (26)$$

with the parameters given in Table 2.

The cross section $\sigma_{soft}^{\gamma^* \gamma^*}(Q^2, P^2)$ obtained by the continuation of the above,

$$\sigma_{soft}^{\gamma^* p} = \frac{4\pi^2 \alpha_{em}}{Q^2} f_{soft}(Q^2),$$

into the Q^2, P^2-plane reads

$$\sigma_{soft}^{\gamma^*\gamma^*}(Q^2, P^2) = \frac{\sigma_{soft}^{\gamma\gamma}}{1 + R_{soft}^2(Q^2 + P^2)} \times$$

$$\times \left[1 + c_{soft} \ln \left(1 + \frac{r_{soft}^2 Q^2}{1 + r_{soft}^2 P^2} + \frac{r_{soft}^2 P^2}{1 + r_{soft}^2 Q^2} \right) \right], \quad (27)$$

with the parameters given in Table 2 and the on-shell cross section

$$\sigma_{soft}^{\gamma\gamma} = \frac{(4\pi^2 \alpha_{em} a_{soft} R_{soft}^2)^2}{\sigma_{soft}^{pp}}. \quad (28)$$

A.2. CD BFKL charm eigen-structure function

In practical evaluations, one needs the charm eigen-structure function $f_m^c(Q^2)$. For the rightmost hard BFKL pole, it is given by

$$f_0^c(Q^2) = a_0 \frac{R_0^2 Q^2}{1 + R_0^2 Q^2} \left[1 + c_0 \ln(1 + r_0^2 Q^2) \right]^{\gamma_0}, \quad (29)$$

where $\gamma_0 = 4/3\Delta_0$, while for the subleading hard BFKL poles we have

$$f_m^c(Q^2) = a_m f_0(Q^2) \frac{1 + K_m^2 Q^2}{1 + R_m^2 Q^2} \times$$

$$\times \prod_{i=1}^{m_{max}} \left(1 - \frac{z}{z_m^{(i)}} \right), \quad m \geq 1, \quad (30)$$

where $m_{max} = \min\{m, 2\}$ and

$$z = \left[1 + c_m \ln(1 + r_m^2 Q^2) \right]^{\gamma_m} - 1, \quad \gamma_m = \gamma_0 \delta_m. \quad (31)$$

The parameters tuned to reproduce the numerical results for $f_m^c(Q^2)$ at $Q^2 \lesssim 10^5$ GeV^2 are listed in Table 3.

The soft component of the charm structure function is parameterized as

$$f_{soft}^c(Q^2) = \frac{a_{soft} R_{soft}^2 Q^2}{1 + R_{soft}^2 Q^2} \times$$

$$\times \left[1 + c_{soft} \ln(1 + r_{soft}^2 Q^2) \right], \quad (32)$$

with parameters given by in Table 3.

REFERENCES

1. R. Nisius, Phys. Rep. **332**, 165 (2000).

2. J. Bartels, A. De Roeck, and H. Lotter, Phys. Lett. B **389**, 742 (1996).

3. J. Bartels, C. Ewerz, and R. Staritzbichler, E-Print Archive hep-ph/0004029.

4. S. J. Brodsky, F. Hautmann, and D. E. Soper, Phys. Rev. D **56**, 6957 (1997).

5. M. Boonekamp, A. De Roek, Ch. Royon, and S. Wallon, Nucl. Phys. B **555**, 540 (1999).

6. L3 Coll.: M. Acciarri et al., Phys. Lett. B **436**, 403 (1998).

7. OPAL Coll.: G. Abbiendi et al., Eur. Phys. J. C **14** (2000).

8. L3 Coll.: M. Acciarri et al., Phys. Lett. B **453**, 333 (1999).

9. OPAL Coll.: K. Ackerstaff et al., Phys. Lett. B **412**, 225 (1997).

10. Particle Data Group, Eur. Phys. J. C **3**, 1 (1998).

11. V. M. Budnev, I. F. Ginzburg, G. V. Meledin, and V. G. Serbo, Phys. Rep. **15**, 181 (1975).

12. V. S. Fadin, E. A. Kuraev, and L. N. Lipatov, Phys. Lett. B **60**, 50 (1975); E. A. Kuraev, L. N. Lipatov, and V. S. Fadin, Zh. Eksp. Teor. Fiz. **71**, 840 (1976); **72**, 377 (1977) [Sov. Phys. JETP **44**, 443 (1976); **45**, 199 (1977)].

13. L. N. Lipatov, Zh. Eksp. Teor. Fiz. **90**, 1536 (1986) [Sov. Phys. JETP **63**, 904 (1986)].

14. Ya. Ya. Balitsky and L. N. Lipatov, Yad. Fiz. **28**, 1597 (1978) [Sov. J. Nucl. Phys. **28**, 822 (1978)].

15. V. N. Gribov, B. L. Ioffe, I. Ya. Pomeranchuk, and A. P. Rudik, Zh. Eksp. Teor. Fiz. **42**, 1419 (1962) [Sov. Phys. JETP **16**, 220 (1963)].

16. N. N. Nikolaev, B. G. Zakharov, and V. R. Zoller, Pis'ma Zh. Eksp. Teor. Fiz. **66**, 134 (1997) [JETP Lett. **66**, 138 (1997)].

17. N. N. Nikolaev and V. R. Zoller, Pis'ma Zh. Eksp. Teor. Fiz. **69**, 91, 176 (1999) [JETP Lett. **69**, 103, 187 (1999)].

18. N. N. Nikolaev, J. Speth, and V. R. Zoller, Phys. Lett. B **473**, 157 (2000).

19. N. N. Nikolaev, B. G. Zakharov, and V. R. Zoller, Pis'ma Zh. Eksp. Teor. Fiz. **59**, 8 (1994) [JETP Lett. **59**, 6 (1994)].

20. N. N. Nikolaev, B. G. Zakharov, and V. R. Zoller, Zh. Eksp. Teor. Fiz. **105**, 1498 (1994) [JETP **78**, 806 (1994)].

21. N. N. Nikolaev and B. G. Zakharov, Phys. Lett. B **327**, 149 (1994); **333**, 250 (1994); **327**, 157 (1994).

22. E. M. Levin and M. G. Ryskin, Yad. Fiz. **34**, 1154 (1981) [Sov. J. Nucl. Phys. **34**, 619 (1981)].

23. O. Nachtmann, Ann. Phys. **209**, 436 (1991); H. Dosch and Yu. A. Simonov, Phys. Lett. B **205**, 339 (1988); Yu. A. Simonov, Nucl. Phys. B **324**, 67 (1989); H. Dosch, E. Ferreira, and A. Krämer, Phys. Rev. D **50**, 1992 (1994); P. V. Landshoff and O. Nachtmann, Z. Phys. C **35**, 405 (1987); H. G. Dosch, T. Gousset, G. Kulzinger, and H. J. Pirner, Phys. Rev. D **55**, 2602 (1997); A. Donnachie and P. V. Landshoff, Phys. Lett. B **437**, 408 (1998); K. Golec-Biernat and M. Wüsthoff, Phys. Rev. D **59**, 014017 (1999); U. D'Alesio, A. Metze, and H. J. Pirner, Eur. Phys. J. C **9**, 601 (1999); G. Kulzinger, H. G. Dosch, and H. J. Pirner, Eur. Phys. J. C **7**, 73 (1999).

24. T. F. Walsh and P. M. Zerwas, Phys. Lett. B **44**, 195 (1973); R. L. Kingsley, Nucl. Phys. B **60**, 45 (1973).

25. G. A. Schuler and T. Sjöstrand, Phys. Lett. B **376**, 193 (1996).

26. N. N. Nikolaev and B. G. Zakharov, Z. Phys. C **49**, 607 (1991).

27. J. Nemchik, N. N. Nikolaev, E. Predazzi, B. G. Zakharov, and V. R. Zoller, Zh. Eksp. Teor. Fiz. **113**, (1998) [JETP **86**, 1054 (1998)].